Journal of Peptide Science
J. Peptide Sci. **7**: 521–528 (2001)
DOI: 10.1002/psc.348

A Bioactive Somatostatin Analog without a Type II′ β-Turn: Synthesis and Conformational Analysis in Solution

SHAOKAI JIANG[a], SHARON GAZAL[b], GARY GELERMAN[c], OFER ZIV[c], OLGA KARPOV[c], PNINIT LITMAN[c], MOSHE BRACHA[c], MICHAEL AFARGAN[c], CHAIM GILON[b,*] and MURRAY GOODMAN[a,*]

[a] Department of Chemistry and Biochemistry, University of California, San Diego, La Jolla, CA, USA
[b] Department of Organic Chemistry, Hebrew University, Jerusalem, Israel
[c] Peptor Ltd., Kiryat Weizmann, Rehovot, Israel

Received 27 February 2001
Accepted 11 May 2001

Abstract: A cyclic somatostatin analog H-Cys[1]-Phe[2]-Trp[3]-D-Trp[4]-Lys[5]-Thr[6]-Phe[7]- N-Gly[8]-NH_2 (S-S-$[CH_2]_2$ bridge) (**1**) has been synthesized. Biological assays show that this compound has strong binding affinities to somatostatin hsst2 and hsst5 receptor subtypes (5.2 and 1.2 nM, respectively, and modest affinity to hsst4 (41.1 nM)). Our conformational analysis carried out in DMSO-d_6 indicates that this compound exists as two structures arising from the *trans* and *cis* configurations of the peptide bond between Phe[7] and *N*-alkylated Gly[8]. However, neither conformer exhibits a type II′ β-turn. This is the first report of a potent bioactive somatostatin analog that does not exhibit a type II′ β-turn in solution. Molecular dynamics simulations (500 ps) carried out at 300 K indicate that the backbone of compound **1** is more flexible than other cyclic somatostatin analogs formed by disulfide bonds. Copyright © 2001 European Peptide Society and John Wiley & Sons, Ltd.

Keywords: conformation; NMR; somatostatin; β-turn

INTRODUCTION

Somatostatin, a cyclic tetradecapeptide hormone, known for its ability to inhibit the release of growth hormone, was isolated from ovine hypothalamus in 1973 [1]. Somatostatin also suppresses the release of many other bioactive molecules, including glucagon, insulin, gastrin and secretin [2–4]. Owing to its distribution in the central nervous system and spinal cord, somatostatin may also play a role in neural transmission [5,6].

Because of somatostatin's wide range of physiological roles and clinical applications, extensive studies have been carried out to investigate the structure-activity relationships of analogs. Research results indicate that the tetrapeptide segment, Ph[3]-D-Trp[4]-Lys[5]-Thr[6], plays a very important role in the bioactivity of somatostatin analogs. Conformational analysis shows that this tetrapeptide segment forms a type II′ β-turn which is stabilized by a hydrogen bond between the NH of Thr[6] and the C=O of Phe[3] [7–10]. The type II′ β-turn aligns the side chains of D-Trp[4] and Lys[5] closely to each other in the $i+2$ and $i+3$ positions, respectively [9,11–13]. These features constitute the structural and conformational requirements for somatostatin analog binding affinity. However, some NMR data suggest that structures other than the β-turn are observed [14–17]. The X-ray crystallographic studies on sandostatin (a potent disulfide analog used in the clinic) have demonstrated that this molecule adopts three β-turn conformations in the crystalline state [18]. In this paper we report the

Abbreviations: DQF-COSY, double-quantum-filtered correlated spectroscopy; MBHA, 4-methylbenzhydrylamine; NMP, *N*-methylpyrrolidone; PyBroP, bromo-tris-pyrrolidino-phosphonium hexafluorophosphate; TIS, triisopropylsilane.

* Correspondence to: M. Goodman, Department of Chemistry and Biochemistry, University of California, San Diego, La Jolla, CA, USA; e-mail: mgoodman@ucsd.edu
* Correspondence to: C. Gilon, Department of Organic Chemistry. Hebrew University, Jerusalem, Israel: e-mail: gilon@vms.juji.ac.il

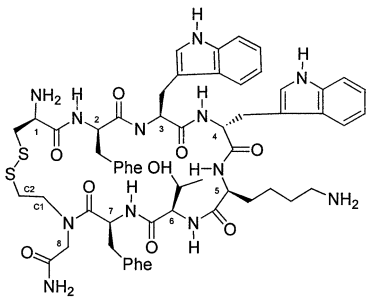

Figure 1 The chemical structure of compound **1**:

H-Cys[1]-Phe[2]-Trp[3]-D-Trp[4]-Lys[5]-Thr[6]-Phe[7]- N-Gly[8]-NH$_2$

S-S-[CH$_2$]$_2$

synthesis and conformations of compound **1** (Figure 1). Cyclization of the octapeptide was accomplished through the formation of a disulfide bond between Cys[1] and thioethyl-*N*-alkylated Gly[8]. This analog is active, with a binding affinity for sst2 and sst5 receptor subtypes of 5.2 and 1.2 nM, respectively, and is metabolically stable ($t_{1/2} > 3$ h) when exposed to a renal homogenate.

MATERIALS AND METHODS

Synthesis of Compound 1

Rink amide MBHA resin (1.5 g, 0.55 mmol/g) was pre-swollen for 2 h in NMP while shaking in a reaction vessel equipped with a sintered glass bottom. The Fmoc protecting group was removed from the resin by reaction with 20% piperidine in NMP (2×30 min) and the resin was washed with NMP (5×2 min) and DCM (2×2 min). The Fmoc removal was monitored by the qualitative ninhydrin (Kaiser) test [19]. A coupling cycle was carried out with Fmoc-N^{α}-[ω(Acm)-S-Et]Gly-OH (3 eq.), PyBroP (3 eq.), and DIEA (7 eq.) in NMP for 2 h at room temperature after preactivation for 10 min. Following coupling, the peptidyl-resin was washed with NMP (5×2 min) and DCM (2×2 min). The completion of reaction was monitored by the ninhydrin test. Capping of the unreacted resin amines was carried out by reaction of the peptidyl-resin with acetic anhydride (0.5 M), DIEA (0.125 M) and HOBt (0.015 M) in DMF for 30 min at room temperature. After capping, NMP and DCM washes were carried out as above.

Deprotection, coupling, ninhydrin tests and washes for peptide elongation to the octapeptide were completed as described above.

After coupling of Fmoc-Cys(Acm)-OH, the resin was dried and cyclization was carried out on 750 mg of peptidyl-resin using iodine (10 eq.) in DMF:H_2O (4:1) at room temperature for 40 min. The peptidyl-resin was washed with DMF (2×2 min), 2% ascorbic acid in DMF (2×2 min), NMP (5×2 min) and DCM (2×2 min). Following Fmoc removal the peptidyl-resin was washed with NMP (5×2 min) and DCM (2×2 min). The peptide was cleaved from the resin and deprotected by reaction with TFA (95%), TIS (2.5%) and H_2O (2.5%) at 0°C for 0.5 h and for 2.5 h at room temperature. The resin was removed by filtration.

The solvent from the filtrate was removed under nitrogen. The oily product obtained was triturated with cold ether and the ether was then decanted. The precipitate was washed with cold ether several times yielding 190 mg (41% yield) of a white powder. Analytical HPLC: RP18 Vydac 4×250 mm; flow: 1 mL/min; $T = 35$°C; detection UV 215 nm; gradient: A = 0.1% TFA in TDW, B = 0.1% TFA in CH_3CN, 0 min 90:10, 1 min 90:10, 30 min 37:63, 35 min 10:90, 40 min 10:90; $R_T = 19.25$ min. MS: (ES VG-Platform II) m/z calc. 1131.2, obs. 1131.4 $[MH]^+$.

The crude peptide was purified by reversed-phase preparative HPLC. Fractions were analyzed by analytical HPLC-MS. The product was obtained by lyophilization of the desired fraction, which eluted as a single peak in analytical HPLC. Amino acid analysis of the hydrolyzed peptide showed the correct amino acid composition (except for Cys).

NMR

The NMR experiments were carried out in DMSO-d_6. The sample was prepared by dissolving compound **1** in 0.50 ml DMSO-d_6 at a concentration of about 5 mM. All NMR experiments were performed on a 500 MHz Bruker AMX500 spectrometer at 300 K. Various 1D spectra were acquired from 300 to 320 K to measure the temperature coefficients of the amide protons. The 2D-NMR spectra were recorded in phase-sensitive mode using time-proportional phase increment (TPPI) or States-TPPI [20] in $\omega 1$ dimension and quadrature detection was used in both dimensions. Double quantum filtered COSY (DQF-COSY) spectra were acquired with the pulse sequence of Derome *et al.* [21]. The TOCSY spectra were obtained using the MLEV-17 spin lock sequence [22] with mixing time of 35 and 75 ms, respectively. The off-resonance ROESY experiment with adiabatic trapezoidal pulse ($\theta = 54.7°$) [23] was used to obtain NOE data instead of the traditional

ROESY in order to eliminate the off-resonance effects and scalar correlations [24]. The mixing times were 150 and 250 ms, respectively. All spectra were collected with 2048 data points in $\omega 2$ and 456–512 $\omega 1$ increments and zero-filled to 2048×1024 data points during the data processing. The DQF-COSY experiment was obtained using 4096×512 data points and processed with 4096×1024 data points. Chemical shifts were referenced to DMSO-d_6 (2.49 ppm). The coupling constants were obtained from 1D ^{1}H-NMR and 2D DQF-COSY spectra. The NOE cross-peak volumes were calibrated against the distance between the two β-protons of Lys^5 in each conformer on the basis of isolated spin pair approximation (ISPA) [25]. The restraints were classified as strong, medium and weak with distance upper limits of 2.5, 3.5 and 4.5 Å, respectively.

Molecular Modeling

The crude structures were generated from the distance geometry program, DGII, using the distance restraints derived from NOE intensities. These structures were subjected to restrained minimization. The ϕ torsion angles derived from a Karplus-type equation [26] and hydrogen bonding pattern (if observed) of these DGII structures, were compared with the values derived from NMR data. For the ϕ torsion angles, an error range of $\pm 30°$ was tolerated. The hydrogen bonded structures in which amide protons exhibited a temperature coefficient < -22 pp/K [27] were retained. Structures which were not consistent with the experimental data (including torsion angles and temperature coefficients) were discarded. The remaining structures were subjected to restrained dynamics simulations.

Restrained molecular dynamics simulations were carried out *in vacuo* employing the DISCOVER (Version 98.0) program [28] with the CFF91 force field. The NOE restraints were included with a force constant of 15 kcal/mol (Å^2). A distance-dependent dielectric constant was used to take into account the solvent effect [29]. No cross-terms or Morse terms were used in the force field.

Prior to every restrained dynamics simulation, the system was equilibrated with 3 ps of initialized dynamics calculations. After that period, the selected DGII structures were submitted to 10 ps of molecular dynamics at 1000 K with a step size of 1 fs. At regular intervals of 1 ps, conformations were extracted and subjected to a preliminary energy minimization by the steepest descent method, until the maximum derivative was less than 1 kcal/mol. Starting from each of these minimized structures, a further 10 ps of molecular dynamics was carried out at 300 K. Again, at regular intervals of 1 ps, unrestrained minimization was performed to generate ensembles of minimized structures with the VA09A algorithm so that the maximum derivative was less than 0.01 kcal/mol.

The molecular dynamics simulations led to 100 minimized structures for each structure selected from DGII calculation. The resulting conformations were then examined and selected according to their consistency with the NOE, $^3J_{\alpha H \sim NH}$ coupling constants and hydrogen bonding patterns. Those structures consistent with the experimental results and with energies not higher than 10 kcal/mol [30] compared to the lowest energy were selected for cluster analysis [31] to obtain the predominant molecular conformations in solution.

RESULTS AND DISCUSSION

Based on 2D TOCSY, DQF-COSY, DQF-COSY and ROESY spectra, the main-chain protons were assigned. The aromatic ring protons were not resolvable because of chemical shift overlap in this region. Residues 4–8 exhibited two sets of signals, indicating the presence of both the *cis* and *trans* configurations between Phe^7 and *N*-alkylated Gly^8. (For clarity, the *cis* and *trans* arrangements around Phe^7 and *N*-alkylated Gly^8 are denoted as configurations in the present text.) The chemical shifts and distance constraints for backbone and side-chain protons of the two conformers derived from NOE intensities are listed in Tables 1–3.

Following the protocol of structural determination in solution, two main conformations of compound **1** in DMSO-d_6 were proposed and are shown in Plates 1 and 2. Although mono-conformational analysis is not accurate to elucidate all of the NMR data for small molecules in solution, the approach is helpful in focusing on the highly populated conformation of the molecule.

For conformer A, a total of 400 structures were generated from the restrained dynamics simulations with an energy range of 266–300 kcal/mol. Of those, 148 structures exhibited energies smaller than 277 kcal/mol. The low energy structures were categorized into eleven clusters according to their dihedral angles. The final structure was selected from the most populated clusters with particular reference to the NMR data. The dihedral angles (ϕ, ψ) are listed in Table 4. The *N*-terminal residues

Table 1 Proton Chemical Shifts of Compound **1** in DMSO-d_6 (ppm)

Residue	Proton	Conformer	
		A	B
Cys[1]	NH	8.54	8.54
	α	4.48	4.48
	β	3.08/2.75	3.08/2.75
Phe[2]	NH	8.42	8.42
	α	4.48	4.48
	β	2.83/2.64	2.83/2.64
Trp[3]	NH	8.25	8.25
	α	4.40	4.40
	β	2.85/2.72	2.85/2.82
D-Trp[4]	NH	8.30	8.42
	α	4.49	4.55
	β	3.03/2.89	3.08/2.83
Lys[5]	NH	8.05	7.98
	α	4.14	4.24
	β	1.57/1.38	1.65/1.40
	γ	0.99	1.10
Thr[6]	NH	7.41	7.62
	α	4.24	4.03
	β	3.98	3.89
Phe[7]	NH	8.24	7.78
	α	4.86	4.66
	β	3.06/2.91	2.94/2.82
Gly[8]	$\alpha 2$	3.86	4.45
	$\alpha 1$	3.78	3.84
NCH_2CH_2S			
	H_{11}/H_{12}	3.50/3.45	3.53/3.48
	H_{21}/H_{22}	2.84/2.62	2.86/2.63

(Cys[1] and Phe[2]) were not included in the Table because their NOE data could not be differentiated between conformer A and conformer B.

Conformer A is stabilized by a hydrogen bond between the Thr[6] NH and the Phe[2] C=O spanning Trp[3], D-Trp[4] and Lys[5] residues. An α-helical turn [32] is formed in this region. The structure was confirmed by the relatively strong $\alpha H^4 \sim NH^5$, medium $NH^4 \sim NH^5$, $NH^5 \sim NH^6$ NOE correlations and weak $NH^4 \sim NH^6$ NOE in DMSO-d_6 (Table 2). The low temperature coefficient of the amide proton of residue Thr[6] in DMSO-d_6 (Table 5) shows that this proton is involved in hydrogen bonding. Only the hydrogen bond formed between the Thr[6] NH and the Phe[2] C=O satisfies most of the backbone

Table 2 Summary of the Observed Backbone NOEs in DMSO-d_6

NOE	Conformer	
	A	B
$\alpha H^2 \sim NH^3$	m-s	m-s
$\alpha H^3 \sim NH^3$	m	m
$\alpha H^3 \sim NH^4$	w	s
$\alpha H^4 \sim NH^4$	s	m
$NH^4 \sim NH^5$	m-w	w
$NH^4 \sim NH^6$	w	[a]
$\alpha H^4 \sim NH^5$	m-s	s
$\alpha H^5 \sim NH^5$	m	m-w
$\alpha H^5 \sim NH^6$	m	s
$NH^5 \sim NH^6$	m	[a]
$\alpha H^6 \sim NH^6$	m	m
$\alpha H^6 \sim NH^7$	s	m-s
$\alpha H^7 \sim NH^7$	m	m
$NH^6 \sim NH^7$	m-w	[a]
$\alpha H^7 \sim N1^8$	[a]	m-w
$\alpha H^7 \sim N2^8$	[a]	s
$\alpha H^7 \sim H11$	m-s	[a]
$\alpha H^7 \sim H12$	m-w	[a]
$\alpha H^7 \sim H21$	m-w	[a]
$\alpha H^7 \sim H22$	s	[a]

[a] NOE not found.

NOE restraints (with two violations no larger than 0.3 Å). Unlike the previously reported somatostatin analogs [8–12,17,33,34], the backbone of the *N*-terminal (Cys[1], Phe[2]) residues are out of the plane formed by the backbone of Trp[3]-D-Trp[4]-Lys[5]-Thr[6] (Plate 1). However, the backbone of Thr[6] and Phe[3] adopts an extended conformation which is supported by the strong sequential $\alpha H^6 \sim NH^7$ NOE (Table 2) and the large (< 7.7 Hz) $^3J_{NH \sim \alpha H}$ coupling constants (Table 6) of these residues. In addition, the low temperature coefficients measured for the D-Trp[4] ad Lys[5] amide protons (-2.3 and -2.5 ppb/K, respectively) are consistent with the low solvent exposure expected for these amide protons within the structure. The *trans* configuration of the amide bond was supported by the medium to strong NOEs (Table 2) between the α-proton of Phe[7] and the $-NCH_2CH_2S-$ protons.

For conformer B, 300 structures were obtained from restrained dynamics simulations, with an energy range of 258–300 kcal/mol. There are 120 structures with energies less than 269 kcal/mol. The final structure was chosen from a cluster of 38 structures. Their dihedral angles are summarized in Table 4. Again, the *N*-terminal residues (Cys[1] and

Table 3 Summary of the Observed Side-Chain NOEs in DMSO-d_6

Residue	Conformer	
	A	B
Phe[2]		
NH ~ βH_1	W	w
NH ~ βH_2	m-s	m-s
$\alpha H \sim \beta H_1$	NA[a]	NA[a]
$\alpha H \sim \beta H_2$	NA[a]	NA[a]
Trp[3]		
NH ~ βH_1	m-s	m
NH ~ βH_2	m-w	m-w
$\alpha H \sim \beta H_1$	m-w	NA[a]
$\alpha H \sim \beta H_2$	m-s	m-s
D-Trp[4]		
NH ~ βH_1	s	s
NH ~ βH_2	m-w	[b]
$\alpha H \sim \beta H_1$	m	m
$\alpha H \sim \beta H_2$	m	s
Lys[5]		
NH ~ βH_1	s	m-s
NH ~ βH_2	m-w	[b]
$\alpha H \sim \beta H_1$	m-s	s
$\alpha H \sim \beta H_2$	s	s
Phe[7]		
NH ~ βH_1	s	s
NH ~ βH_2	m	w
$\alpha H \sim \beta H_1$	m	m-s
$\alpha H \sim \beta H_2$	m	s

[a] NOE not assignable.
[b] NOE not found.

Phe[2]) were excluded from the table because their NOEs do not distinguish between conformers A and B.

In conformer B the NOE correlations between the α-protons of Phe[7] and Gly[8] (Table 2) indicate that the amide bond between Phe[7] and *N*-alkylated Gly[8] is in a *cis* configuration. There is no hydrogen bond between the NH of Lys[5] and C=O of Phe[2] in spite of the existence of a weak NOE between the NH of D-Trp[4] and Lys[5]. Instead, a γ-turn [35] about D-Trp[4] ($\phi = 75°$, $\psi = -86°$) is observed which is supported by the relatively low temperature coefficient of the Lys[5] amide proton in this conformer. Only one backbone restraint was violated for the structure with less than a 0.5-Å deviation.

The NMR differences for the backbone H's between this compound and other somatostatin analogs such as sandostatin [8–12,17,33,34] are listed in Table 7. The table shows that the conformational features of compound 1 are quite different from those of the other previously reported somatostatin analogs. In conformer A of compound **1** there are continued sequential NH ~ NH NOEs among Trp[4], Lys[5] and Thr[6], as well as $NH^4 \sim NH^6$ NOES. However, in analogs with a type II′ β-turn, the NOE was found only between Lys[5] and Thr[6]. In conformer B, the NH ~ NH NOE was found between D-Trp[4] and Lys[5], instead of Lys[5] and Thr[6]. Another very important difference between compound **1** and the others is the NOE of the αH ~ NH of D-Trp[4]. In analogs with a type II′ β-turn the intensity of this NOE is in the medium range, but in conformer A of compound **1** this NOE is very strong. This demonstrates that the αH and NH are in the same plane. Therefore, the amide proton of Thr[6] is involved in a hydrogen bond with Phe[2] instead of Trp[3]. In conformer B the $\alpha H^5 \sim NH^6$ NOE is very strong while in analogs with type II′ β-turn this NOE is usually in the medium range. The temperature coefficients of amide protons in conformer B were relatively high (< 3 ppb/K) except the of Lys[5], showing the NH of Lys[5] may be involved in a γ-turn hydrogen bond [27].

Although neither conformer of this compound exhibits a type II′ β-turn, the topology of the backbone of conformer B is very similar to the backbone of the

Table 4 Typical Dihedral Angles for Preferred Conformations of Conformer A and B

Residue	Conformer A		Conformer B	
	ϕ (°)	ψ (°)	ϕ (°)	ψ (°)
Trp[3]	-52 ± 25	-35 ± 25	-100 ± 15	87 ± 10
D-Trp[4]	-56 ± 15	-40 ± 25	75 ± 13	-86 ± 26
Lys[5]	-110 ± 30	-53 ± 14	-120 ± 30	95 ± 15
Thr[6]	-165 ± 10	124 ± 17	-150 ± 10	-70 ± 5
Phe[7]	-125 ± 13	95 ± 20	140 ± 5	-125 ± 30

Table 5 Temperature Coefficients of NH Protons in DMSO-d_6 (ppb/K)

	Cys[1]	Phe[2]	Trp[3]	d-Trp[4]	Lys[5]	Thr[6]	Phe[7]
Conformer A	3.0	4.0	3.0	2.3	2.5	0.9	4.5
Conformer B	3.0	4.0	3.0	3.6	2.5	3.0	3.5

Table 6 $J_{\alpha H\sim NH}$ Coupling and the Calculated ϕ Dihedral Angles in DMSO-d_6

Residue	Conformer A		Conformer B	
	$J_{\alpha H\sim NH}$ (Hz)	ϕ (°)	$J_{\alpha H\sim NH}$ (Hz)	ϕ (°)
Phe[2]	7.5	45, 75, −88, −152	7.0	40, 80, −85, −155
Trp[3]	6.3	33, 87, −80, −159	6.2	32, 88, −80, −160
D-Trp[4]	5.8	77, 163, −29, −91	4.0	66, 174
Lys[5]	8.1	−148, −93	7.8	50, 69, −90, −150
Thr[6]	8.2	−146, −94	7.4	44, 76, −88, −152
Phe[7]	7.8	50, 69, −90, −150	7.4	44, 76, −88, −152

[3]$J_{\alpha H\text{-}NH}$ values are within ± 0.5 Hz.
ϕ values were calculated according to: $J = A\cos^2|\phi \pm 60°| + B\cos|\phi \pm 60°| + C$, where + is for D-configuration residues and − for L-configuration residues, $(A, B, C) = (8.6, 1.0, 0.4)$ as proposed by Bystrov [36] for a chiral residue.

Table 7 Comparison of NMR Results for Compound **1** and Sandostatin

Compound **1**		Sandostatin[a]
Conformer A	Conformer B	
NH∼NH NOE: D-Trp[4]∼Lys[5] (m), Lys[5]∼Thr[6] (m), D-Trp[4]∼Thr[6] (w)	NH∼NH NOE: D-Trp[4]∼Lys[5] (w)	NH∼NH NOE: Lys[5]∼Thr[6] (m)
αH∼NH NOE: D-Trp[4]∼D-Trp[4] (s)	αH∼NH NOE: Lys[5]∼Thr[6] (s)	αH∼NH NOE: D-Trp[4]∼D-Trp[4] (m), Lys[5]∼Thr[6] (m)
$\Delta\delta/\Delta T$ of NH: Thr[6]: −0.9 ppb/K	$\Delta\delta/\Delta T$ of NH: Thr[6]: −3.0 ppb/K, Lys[5]: −2.5 ppb/K	$\Delta\delta/\Delta T$ of NH: Thr[6]: < −2.0 ppb/K

[a] Reference [10].

compounds with a type II′ β-turn. Plate 3 shows the overlayed topology of the backbones of conformer B compared with a structure in a standard type II′ β-turn which was built using the 'Biopolymer' module of the InsightII package.

In order to study the dynamics of conformer B of compound **1**, 500 ps of molecular dynamics simulations were performed at 300 K. The dynamics simulation shows the backbone of this compound to be much more flexible than those of the analogs with a type II′ β-turn. None of the individual simulated structures are fully consistent with all of the NOE constraints. The trajectories of conformer B extracted from dynamics simulations are shown in Plate 4.

The side-chain orientations of compound **1** were analyzed according to the relative NOE intensities between the NH and the β-protons as well as the αH and β-protons. In both conformers A and B, the D-Trp[4] and Lys[5] residues are *trans* (*t*) and *gauche* (g^+), respectively, and the side chains of Trip[4] and Lys[5] are not parallel to each other. This conclusion was supported by the lack of a high field chemical shift for the γH of Lys[5] (Table 1). This shows the γH of Lys[5] is not influenced by the shielding effects of the aromatic ring of D-Trp[4] as previously reported [9,13]. The aromatic side-chain orientations of Trp[3] and Phe[2] could not be solved because of the overlap of their chemical shifts. The side chain of Phe[7] is

predominantly *trans* as has been shown in other studies [11].

CONCLUSIONS

The conformations of compound **1** were studied in DMSO solution. This somatostatin analog shows two sets of NMR signals from D-Trp^4 to the *N*-alkylated Gly^8 because of the *cis* and *trans* conformations of the peptide bond between Phe^7 and Gly^8. Unlike other somatostatin analogs, this molecule does not exhibit a type II′ β-turn in either conformer. The basis for the difference between compound **1** and other somatostatin analogs arises from the disulfide 'bridging region' [7] of Cys^1 and thioether-*N*-alkylated Gly^8. This region maintains the side chain orientation of the tetrapeptide, L-Trp^3-D-Trp^4-Lys^5-Thr^6, but its backbone is not a type II′ β-turn. However, the overall backbone topology of conformer B is similar to that of somatostatin analogs with a type II′ β-turn.

Compound **1** has the essential pharmacophores required for the activity of somatostatin analogs, namely D-Trp^4 and Lys^5. The striking similarity of the backbone topology between compound **1** and somatostatin analogs with a type II′ β-turn indicates that the pharmacophores and the backbone topology, not the type II′ β-turn about the Phe-D-Trp-Lys-Thr segment, is essential for the activity of somatostatin analogs. Because of backbone flexibility, the receptor-bound conformation of compound **1** could be similar to other somatostatin analogs with a type II′ β-turn.

Acknowledgements

We wish to thank the National Institute of Health (DK15410) for its financial support and Audrey Kelleman for her critical review of the manuscript.

REFERENCES

1. Brazeau P, Vale W, Burgus R, Ling N, Bucher M, River J, Guillemin R. Hypothalamic polypeptide that inhibits the secretion of the immunoreactive pituitary growth hormone. *Science* 1973; **179**: 77–79.
2. Koerker DJ, Harker LA, Goodner CJ. Effects of somatostatin on hemostasis in baboons. *New Engl. J. Med.* 1975; **293**: 476–479.
3. Gerich JE, Lovinger R, Grodsky GM. Inhibition by somatostatin of glucagon and insulin release from the perfused rat pancreas in response to arginine, isoproterenol, and theophyline. Evidence for a preferential effect on glucagon secretion. *Endocrinology* 1975; **96**: 749–754.
4. Johansson C, Wisen O, Efendic S, Uvnaes-Wallensten K. Effects of somatostatin on gastrointestinal propagation and adsorption of oral glucose in man. *Digestion* 1981; **22**: 126–137.
5. Iversen LL. Non-opioid neuropeptides in mammalian CNS. *Annu. Rev. Pharmacol. Toxicol.* 1983; **23**: 1–27.
6. Seybold VS, Hylden JLK, Wilcox GL. Intrathecal substance P and somatostatin in rats: behaviors indicative of sensation. *Peptides* 1982; **3**: 49–54.
7. Nutt RF, Saperstein R, Veber DF. Structural and conformational studies regarding trytophan in a cyclic hexapeptide somatostatin analog. In *Peptides: Structure and Function*, Hruby VJ, Rich DH (eds). Pierce Chemical Company: Rockford, IL, 1983; 345–348.
8. Veber DF. Design and discovery in the development of peptide analogs. In *Peptides: Chemistry and Biology*, Smith JA, Rivier JE (eds). ESCOM: Leiden, 1992; 3–14.
9. Freidinger RM, Perlow DS, Randall WC, Saperstein R, Arison BH, Weber DF. Conformational modifications of cyclic hexapeptide somatostatin analogs. *Int. J. Pept. Protein Res.* 1984; **23**: 142–150.
10. Melacini G, Zhu Q, Osapay G, Goodman M. A refined model for the somatostatin pharmacophore. Conformational analysis of lanthionine-sandostatin analogs. *J. Med. Chem.* 1997; **40**: 2252–2258.
11. Huang Z, He YB, Raynor K, Tallent M, Reisine T, Goodman M. Main-chain and side-chain chiral methylated somatostatin analogs: synthesis and conformational analyses. *J. Am. Chem. Soc.* 1992; **114**: 9390–9401.
12. He YB, Huang Z, Raynor K, Tallent M, Reisine T, Goodman M. Synthesis and conformations of somatostatin-related cyclic hexapeptides incorporating specific α- and β-methylated residues. *J. Am. Chem. Soc.* 1993; **115**: 8066–8072.
13. Arison BH, Hirschmann R, Veber DF. Inferences about the conformation of somatostatin at a biologic receptor based on NMR studies. *Bioorg. Chem.* 1978; **7**: 447–451.
14. Wynants C, Van Binst G, Loosli HR. SMS 2010995, a very potent analog of somatostatin. Assignment of the proton 500 MHz n.m.r. spectra and conformational analysis in aqueous solution. *Int. J. Pept. Protein Res.* 1985; **25**: 608–614.
15. Wynants C, Van Binst G, Loosli HR. SMS 201-995, an octapeptide somatostatin analog. Assignment of the proton 500 MHz n.m.r. spectra and conformational analysis of SMS 201-995 in dimethylsulfoxide. *Int. J. Pept. Protein Res.* 1985; **25**: 615–621.
16. Wynants C, Tourwe D, Kazmierski W, Hruby VJ, Van Binst G. Conformation of two somatostatin analogs in

aqueous solution. Study by NMR methods and circular dichroism. *Eur. J. Biochem.* 1989; **185**: 371–381.
17. Melacini G, Zhu Q, Goodman M. Multiconformational NMR analysis of sandostatin (Octreotide). Equilibrium between β-sheet and partially helical structures. *Biochemistry* 1997; **36**: 1233–1241.
18. Pohl E, Heine A, Sheldrick GM, Dauter Z, Wilson KS, Kallen J, Huber W, Pfaeffli PJ. Structure of Octreotide, a somatostatin analog. *Acta Crystallogr.* 1995; **D51**: 48–59.
19. Stewart JM, Young JD. *Solid Phase Peptide Synthesis* (2nd edn). Pierce Chemical Company: Rockford, IL, 1984.
20. States DJ, Haberkon RA, Ruben DJ. A two-dimensional nuclear Overhauser experiment with pure absorption phase in four Quadrants. *J. Magn. Reson.* 1982; **48**: 286–292.
21. Derome AE, Williamson MP. Rapid-pulsing artifacts in double-quantum-filtered COSY. *J. Magn. Reson.* 1990; **88**: 177–185.
22. Bax A, Davis DG. MLEV-17-based two-dimensional homonuclear magnetization transfer spectroscopy. *J. Magn. Reson.* 1985; **65**: 355–360.
23. Desvaux H, Berthault P, Birlirakis N, Goldman M, Piotto M. Improved versions of off-resonance ROESY. *J. Magn. Reson.* 1995; **A113**: 47–52.
24. Bax A, Davis DG. Practical aspects of two-dimensional transverse NOE spectroscopy. *J. Magn. Reson.* 1985; **63**: 207–213.
25. Neuhaus D, Williamson MP. *The Nuclear Overhauser Effect in Stereochemical and Conformational Analysis*. VCH Publishers, Inc: New York, 1989.
26. Karplus M. Vicinal proton coupling in nuclear magnetic resonance. *J. Am. Chem. Soc.* 1963; **85**: 2870–2871.
27. Kessler H. Peptide conformations. Part 19. Conformation and biological effects of cyclic peptides. *Angew Chem.* 1982; **94**: 509–520.
28. Hagler AT. Theoretical simulation of conformation, energetics, and dynamics of peptides. In *Peptides*, vol. 7, Udenfriends S, Meienhofer J, Hruby VJ (eds). Academic Press: Orlando, FL, 1985; 214–296.
29. Leach AR. *Molecular Modeling: Principles and Applications*. Longman: Harlow, 1996.
30. Kazmierski WM, Ferguson RD, Lipkowski AW, Hruby VJ. A topographical model of μ-opioid and brain somatostatin receptor selective ligand. *Lett. Peptide Sci.* 1995; **2**: 177–181.
31. Said-Nejad OE, Felder ER, Eduard R, Mierke DF, Yamazaki T, Schiller PW, Goodman M. 14-Membered cyclic opioids to dermorphin and their partially retro-inverso modified analogs. *Int. J. Peptide Protein Res.* 1992; **39**: 145–160.
32. IUPAC-IUB. Commission on Biochemical Nomenclature. *Biochemistry* 1970; **9**: 3471–3479.
33. Veber DF. Design of a highly active cyclic hexapeptide analog of somatostatin. In *Peptides: Synthesis, Structure, and Function*, Rich DF, Gross E (eds). Pierce Chemical Company: Rockford, IL, 1981; 685–694.
34. Kessler H, Bernd M, Kogler H, Zarbock J, Soerensen OW, Bodenhausen G, Ernst RR. Peptide conformation. 28. Relayed heteronuclear correlation spectroscopy and conformational analysis of cyclic hexapeptides containing the active sequence of somatostatin. *J. Am. Chem. Soc.* 1983; **105**: 6944–6952.
35. Matthews BW. The γ-turn. Evidence for a new folded conformation in proteins. *Macromolecules* 1972; **5**: 818–819.
36. Bystrov VF. Spin-spin coupling and the conformational states of peptide systems. *Progr. Nuclear Magn. Reson. Spectrosc.* 1976; **10**: 41–81.

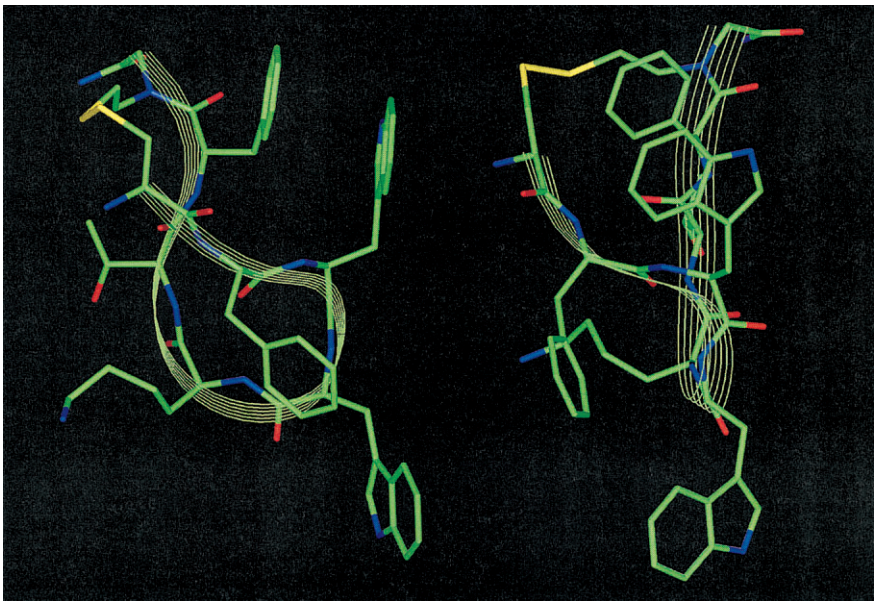

Plate 1 Preferred conformation of conformer A in DMSO-d_6 solution: front view (left), side view (right). The ribbons indicate the backbone orientations.

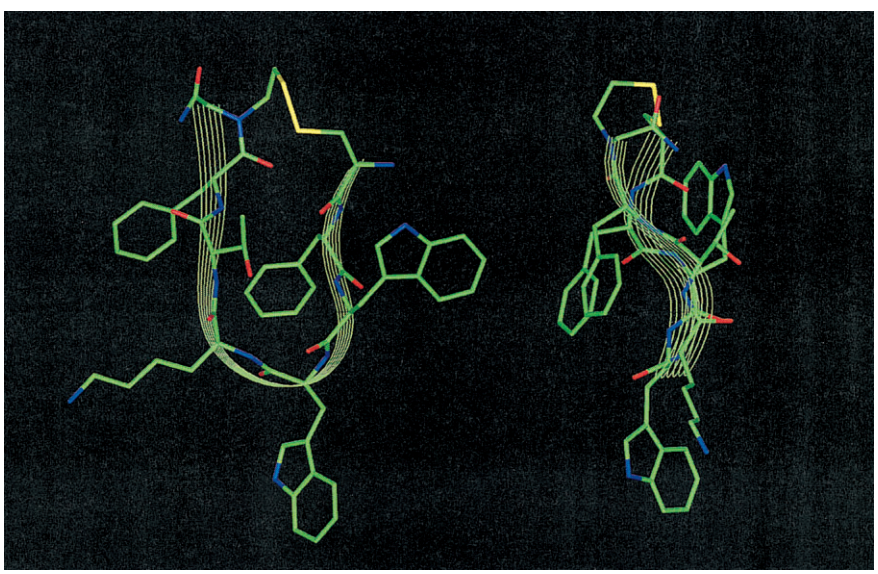

Plate 2 Preferred conformation of conformer B in DMSO-d_6 solution: Front view (left), side view (right). The ribbons indicate the backbone orientations.

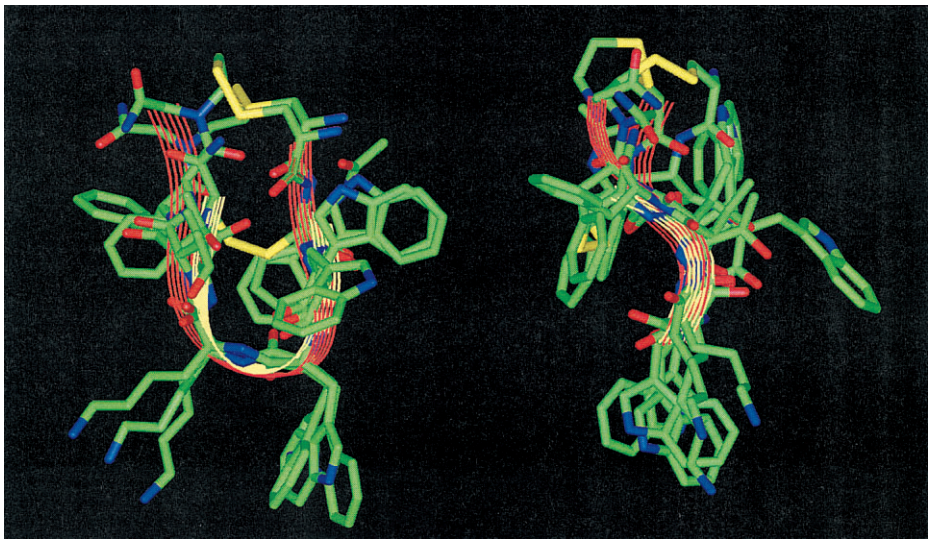

Plate 3 Overlayed plot of the backbone of conformer B with the corresponding backbone conformation of a typical type II′ β-turn: conformer B (red ribbon), reference β-turn analog (yellow ribbon).

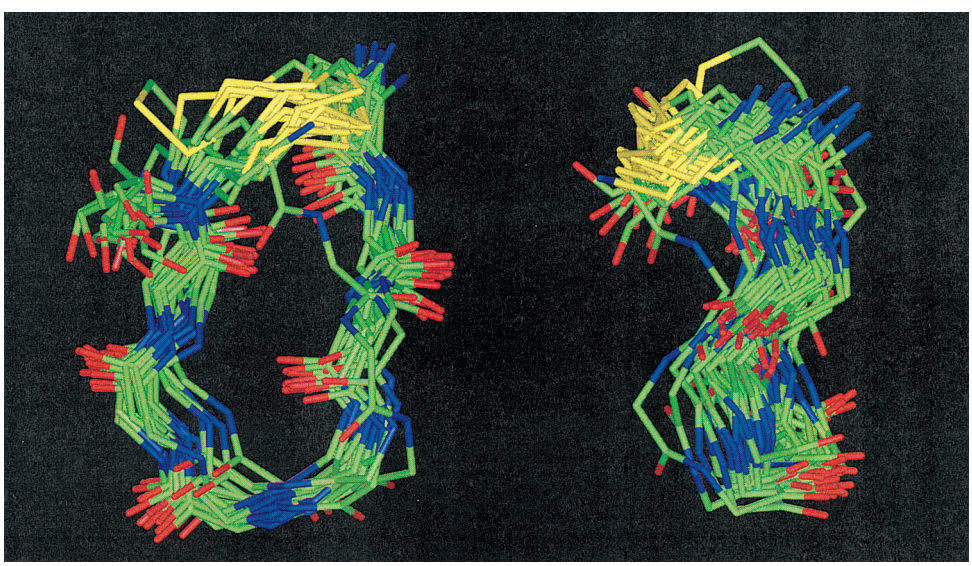

Plate 4 The MD trajectories (every 20 ps) of the backbone atoms from a 500-ps free dynamics simulation of conformer B at 300 K.

